JACS Au
AN OPEN ACCESS JOURNAL OF THE AMERICAN CHEMICAL SOCIETY

pubs.acs.org/jacsau

Article

Stacking of a Cofacially Stacked Iron Phthalocyanine Dimer on Graphite Achieved High Catalytic CH_4 Oxidation Activity Comparable to That of pMMO

Yasuyuki Yamada,* Kentaro Morita, Takuya Sugiura, Yuka Toyoda, Nozomi Mihara, Masanari Nagasaka, Hikaru Takaya, Kiyohisa Tanaka, Takanori Koitaya, Naoki Nakatani, Hiroko Ariga-Miwa, Satoru Takakusagi, Yutaka Hitomi, Toshiji Kudo, Yuta Tsuji, Kazunari Yoshizawa, and Kentaro Tanaka*

Cite This: *JACS Au* 2023, 3, 823–833

Read Online

ACCESS | Metrics & More | Article Recommendations | Supporting Information

ABSTRACT: Numerous biomimetic molecular catalysts inspired by methane monooxygenases (MMOs) that utilize iron or copper-oxo species as key intermediates have been developed. However, the catalytic methane oxidation activities of biomimetic molecule-based catalysts are still much lower than those of MMOs. Herein, we report that the close stacking of a μ-nitrido-bridged iron phthalocyanine dimer onto a graphite surface is effective in achieving high catalytic methane oxidation activity. The activity is almost 50 times higher than that of other potent molecule-based methane oxidation catalysts and comparable to those of certain MMOs, in an aqueous solution containing H_2O_2. It was demonstrated that the graphite-supported μ-nitrido-bridged iron phthalocyanine dimer oxidized methane, even at room temperature. Electrochemical investigation and density functional theory calculations suggested that the stacking of the catalyst onto graphite induced partial charge transfer from the reactive oxo species of the μ-nitrido-bridged iron phthalocyanine dimer and significantly lowered the singly occupied molecular orbital level, thereby facilitating electron transfer from methane to the catalyst in the proton-coupled electron-transfer process. The cofacially stacked structure is advantageous for stable adhesion of the catalyst molecule on the graphite surface in the oxidative reaction condition and for preventing decreases in the oxo-basicity and generation rate of the terminal iron-oxo species. We also demonstrated that the graphite-supported catalyst exhibited appreciably enhanced activity under photoirradiation owing to the photothermal effect.

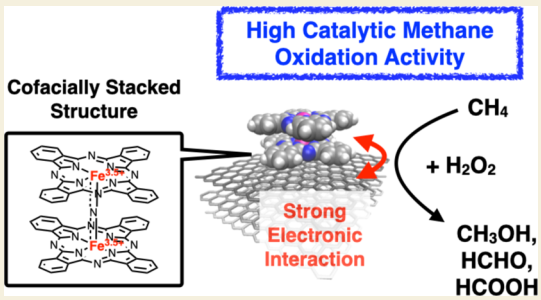

KEYWORDS: *stacking, phthalocyanine, terminal iron-oxo complex, graphite, methane, oxidation, catalysis*

INTRODUCTION

Methane has long been expected to be a next-generation feedstock in the chemical industry because of its abundance in natural gas, shale gas, and methane hydrate. Methane is also efficiently produced from carbon dioxide and hydrogen via the Sabatier process. Methane is, however, a greenhouse gas; hence, from the perspective of decreasing petroleum dependency, preventing global warming, and meeting sustainable development goals (SDGs), the demand for catalysts that can effectively convert methane into more valuable raw chemicals has increased significantly.[1,2] However, efficient catalytic methane conversion under mild reaction conditions has been recognized as a formidable challenge in the field of catalytic science owing to the high C−H bond dissociation energy (104.9 kcal/mol), low polarizability, and negligible electron affinity of methane.

Methane monooxygenases (MMOs) convert methane into methanol under physiological conditions.[3−5] Following the discovery that MMOs utilize iron- or copper-oxo species as catalytic centers (Figure 1a), many researchers have attempted the synthesis of artificial metal complexes by mimicking their reactive centers. Such studies have succeeded in identifying the reactive intermediates and elucidating the reaction mechanism.[5−7] One important process for efficient C−H bond activation of methane is a proton-coupled electron transfer (PCET) pathway (more specifically, hydrogen atom transfer (HAT) or concerted PCET (cPCET)), which can render methane oxidation energetically easier.[8−15] Although there remains discussion, in principle, two important factors for achieving efficient PCET with a catalyst should be considered: (i) positive redox potential for facilitating electron transfer from methane and (ii) higher oxo-basicity to abstract a H atom from methane.[11−19] Despite these insights, the methane

Received: November 15, 2022
Revised: December 29, 2022
Accepted: December 29, 2022
Published: January 10, 2023

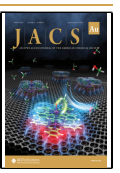

https://doi.org/10.1021/jacsau.2c00618
JACS Au 2023, 3, 823−833

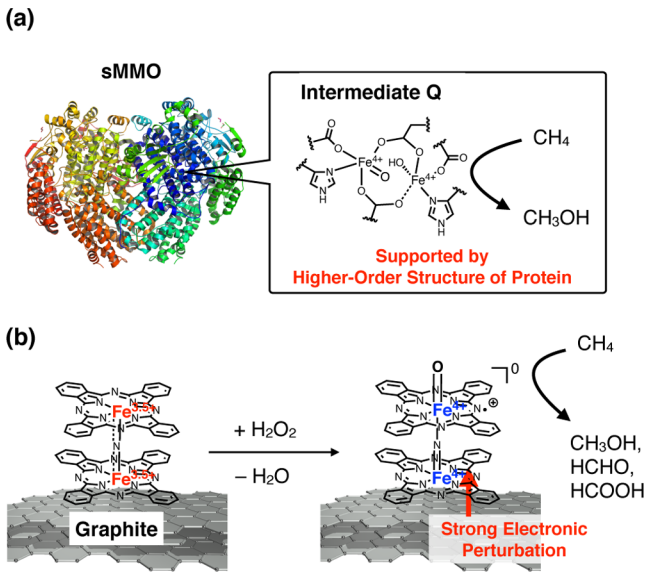

Figure 1. Design of a graphite-supported μ-nitrido-bridged iron phthalocyanine dimer (**1**/G) as an efficient methane oxidation catalyst. (a) High-valent terminal iron-oxo species in a soluble methane monooxygenase (sMMO). (b) Generation of a high-valent terminal iron-oxo species of a graphite-supported μ-nitrido-bridged iron phthalocyanine dimer **1**/G ($\mathbf{1}_{oxo}$/G) for methane oxidation.

oxidation activities of artificial biomimetic molecular catalysts are still orders of magnitude more inferior than those of the natural enzymes.[2,5,20,21] Moreover, most of the artificial molecular oxidation catalysts are unable to sufficiently activate the C−H bond of methane. Considering the high reactivity of MMOs, it would seem that it is possible to improve the activity of artificial molecular catalysts by adopting innovative strategies. In general, natural enzymes enhance the reactivity of their catalytic centers by fine-tuning the electronic structures of the metal centers and coordinating ligands, with the aid of higher order protein structures.[3−5] However, the preparation of artificial systems that mimic such structures requires tremendous synthetic effort. Therefore, it is necessary to develop a facile methodology to dramatically enhance the activity of molecular terminal iron-oxo species in oxidation reactions.

Here, we demonstrate that close-stacking of a μ-nitrido-bridged iron phthalocyanine dimer **1** (Figure 1b) having cofacially stacked structure onto the surface of graphite is a simple and effective strategy for realizing a catalyst with high methane oxidation activity, even rivaling that of natural MMOs. μ-Nitrido-bridged iron porphyrinoid dimers, including μ-nitrido-bridged iron phthalocyanine dimers, are known to be one of the most promising classes of molecular catalysts based on high-valent terminal iron-oxo species for methane oxidation.[22−26,28] Furthermore, peripheral electron-donating alkyl substituents can be introduced into such dimers to improve the catalytic oxidation activity, severalfold.[25,28] However, the probability of achieving high oxo-basicity and positive potential solely through the introduction of substituents is not great because they generally have a trade-off relationship with each other. A novel methodology is required to overcome these limitations.

Our recent study on a supramolecular conjugate based on a μ-nitrido-bridged iron porphyrinoid dimer suggested that the extension of the π-stacked structure, by including an additional porphyrin in the stack, is an effective approach for enhancing its alkane oxidation activity.[26,27] However, the degree of enhancement achieved was not satisfactory. Based on these results, we surmised that the stacked conjugate of a high-valent terminal iron-oxo species of a μ-nitrido-bridged iron phthalocyanine dimer, with no bulky peripheral substituents, onto graphite ($\mathbf{1}_{oxo}$/G, Figure 1b) could result in higher methane oxidation activity. We further deduced that this was due to the strong electronic perturbation, induced by the effective close-stacking of the units $\mathbf{1}_{oxo}$/G, which can be generated by the reaction of an unsubstituted μ-nitrido-bridged iron phthalocyanine dimer on graphite (**1**/G) with H_2O_2 as shown in Figure 1b. Regarding the use of carbon materials for enhanced oxidizing ability, a single graphene-confined iron ion is known to be effective for methane conversion at ambient temperature.[29] In the case of more facile oxidation reactions than methane oxidation, such as phenol oxidation, it has been reported that the adsorption of a catalyst with molecular π-planarity, such as iron porphyrin, onto the surface of graphene can result in enhanced catalytic activity, although the detailed mechanism of the activation is still unclear.[30] In this study, we demonstrated that the cofacially stacked structure of the catalyst molecule is essential for achieving high methane oxidation activity when combining an iron porphyrinoid molecular catalyst and graphite support.

RESULTS AND DISCUSSION

Preparation and Characterization of the Graphite-Supported Catalyst

From a synthetic viewpoint, one difficulty in achieving a closely stacked structure of **1**/G lies in the fact that **1** has very low solubility in many organic solvents because **1** has no peripheral substituents to prevent stacked assemblies forming and, thus, self-aggregation. After a thorough investigation of the reaction conditions, we found that treating graphite with its 1e$^-$-oxidized monocationic complex, $\mathbf{1}^+\cdot I^-$ (the structure is shown in Figure 2a), resulted in the formation of the desired catalyst, **1**/G, in which the neutral form **1** was adsorbed on the graphite surface (Figure 1b). $\mathbf{1}^+\cdot I^-$ has higher solubility in polar organic solvents than **1** because of its ionic characteristic. Pyridine was found to be a good solvent for $\mathbf{1}^+\cdot I^-$ because the axial coordination of pyridine with the Fe center of $\mathbf{1}^+\cdot I^-$ prevents its aggregation.[31,32] Heating a mixture of $\mathbf{1}^+\cdot I^-$ and graphite in pyridine at 80 °C was necessary for the efficient adsorption of **1** onto graphite, which was confirmed by the decolorization of the resulting supernatant (Figure S1). Finally, pyridine that remained on the surface of **1**/G was removed completely by treatment with excess trifluoroacetic acid (TFA).

To characterize the structure of the catalyst on the graphite surface, X-ray photoelectron spectroscopy (XPS) and near-edge X-ray absorption fine structure (NEXAFS) analyses were performed using highly oriented pyrolytic graphite (HOPG) treated with $\mathbf{1}^+\cdot I^-$ (**1**/HOPG). As shown in Figure 2a, after adsorption, the XPS signals corresponding to the iron species in the catalyst shifted slightly to a binding energy that was almost the same as that of **1** (the neutral form), whereas the peaks corresponding to iodine disappeared completely (Figures 2a and S2−S4). This result suggests that $\mathbf{1}^+\cdot I^-$ was reduced by one electron to form neutral complex, **1**, after adsorption onto graphite. The actual catalyst **1**/G (Figures S5 and S6) showed the same XPS spectral characteristics.

https://doi.org/10.1021/jacsau.2c00618
JACS Au 2023, 3, 823−833

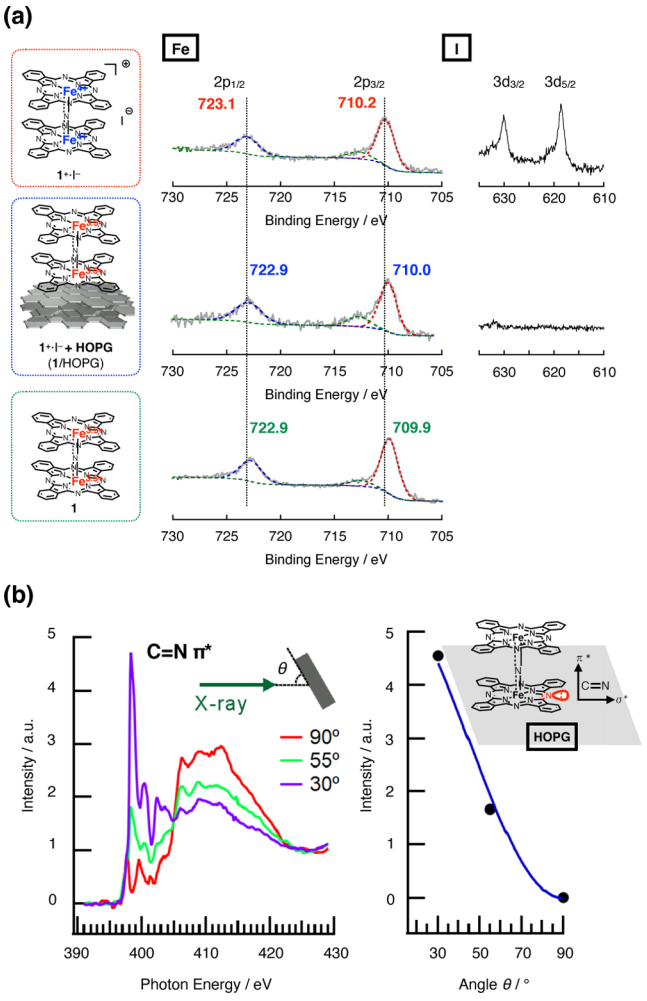

Figure 2. Characterization of a graphite-supported μ-nitrido-bridged iron phthalocyanine dimer (**1**/G). (a) Comparison of Fe 2p and I 3d regions of XPS profiles of a monocationic μ-nitrido-bridged iron phthalocyanine dimer ($\mathbf{1}^{+}\cdot I^{-}$) (upper), a HOPG substrate treated with a pyridine solution of $\mathbf{1}^{+}\cdot I^{-}$ (middle), and $1e^{-}$-reduced species of $\mathbf{1}^{+}\cdot I^{-}$ (**1**) (bottom). The dashed curves are the fitted spectra. The wide scans are shown in Figures S2–S4. (b) Angle-dependent N K-edge NEXAFS spectra of a HOPG substrate adsorbed with the μ-nitrido-bridged iron phthalocyanine dimer (**1**/HOPG). Detailed procedure of the NEXAFS measurement is given in the Supporting Information (page S10).

Moreover, the angle-dependent N K-edge NEXAFS spectrum of **1**/HOPG revealed that **1** was aligned parallel to the graphite surface along its phthalocyanine moiety (Figure 2b). The left part of Figure 2b shows a comparison of the NEXAFS spectra obtained at three different incidence angles of soft X-rays (θ = 90, 55, and 30°) from the HOPG surface. In these spectra, the peaks at 398.2 eV can be assigned to the excitation of the N 1s core electrons to the C=N π^* orbitals of phthalocyanine.[33] Because the C=N π^* transition moment is perpendicular to the phthalocyanine surface, the high intensity of the π^* peak at θ = 30° indicates that the phthalocyanine surface is parallel to the HOPG surface. The right part of Figure 2b shows the incident-angle dependence of the C=N π^* peak intensities with the simulated curve calculated from the tilted angle of the C=N π^* transition moment from the normal of the HOPG surface.[34] As a result of the fitting procedure, the tilt angle of the C=N π^* transition moment was calculated to be 0 from the surface normal, indicating that the phthalocyanine surface was parallel to the HOPG surface. Therefore, these results clearly indicate that **1** was adsorbed onto the π-surface of the HOPG substrate along the π-surface of its phthalocyanine ring (Figure 2b).

Heterogeneous Oxidation of Methane and Ethane

The heterogeneous oxidation of methane, or ethane, was performed in H_2O (3.0 mL) using solid-supported catalyst **1**/G (with 19 μM of **1**), H_2O_2 (189 mM), and TFA (51 mM) under 1.0 MPa gas pressure at 60 °C. The resulting products were analyzed by GC–MS. Significant amounts of oxidized products were detected (Figures 3a, S7 and Tables S1 and S2), indicating that methane, or ethane, was oxidized in a stepwise manner (Figure 3b). The oxidized products were further characterized by ^{1}H-NMR spectroscopy (Figures S8 and S9). In contrast, reactions conducted in the absence of methane (or ethane) yielded much smaller amounts of oxidized products (entries 11 in Tables S1 and S2). The oxidized products observed in the absence of methane or ethane were presumably derived from the organic solvents adsorbed on the solid supports.[26−28] We also performed the oxidation reaction using ^{13}C-labeled methane to confirm that the oxidized products actually originated from methane (Figure S10). As graphite is inherently incapable of oxidizing light alkanes, such as methane or ethane, under these reaction conditions (entry 16 in Table S1), the obtained results clearly imply that the catalyst adsorbed on graphite catalyzed the oxidation of the two alkanes. Moreover, because the reaction could not be quenched by the addition of Na_2SO_3 (Table S2, entry 12), a radical scavenger, the possibility of a Fenton-type reaction was excluded.[28,35−37] Therefore, the actual reactive species should be a high-valent terminal iron-oxo species that is generated in situ.[22−25,28,35−37]

We calculated the effective total turnover number (TTN_{eff}) as an indicator of the catalytic methane and ethane oxidation activity of the catalyst. TTN_{eff} is defined by equations (i) [or (ii)] and (iii) as shown in Figure 3c. In addition, the effective methane conversion number (MCN_{eff}) is defined by equations (iv) and (v). MCN_{eff} indicates the number of methane molecules that a single catalyst molecule can transform, whereas TTN_{eff} reflects the total number of catalytic oxidation reactions. These indicators allow us to compare the catalytic activity of **1**/G with those of natural MMOs and other metal-oxo-based molecular catalysts.

As shown in Figure 3d, the TTN_{eff}s initially increased almost linearly (up to 4 h) in both methane and ethane oxidation reactions, suggesting that the reaction center of **1** retained its catalytic activity under the experimental conditions employed in this work. The excellent stability of **1**/G was confirmed by the fact that the TTN_{eff} in the oxidation of ethanol (3.0 M) reached 30,000 after 1 h of reacting under the same reaction conditions (Table S2, entry 13). We also confirmed that the graphite support of **1**/G was not decomposed into CO_2 or HCOOH significantly during the oxidation reaction (see Supporting Information pages S17 and 18 and entry 11 in Table S1). The gradual decrease in the reaction rate after 4 h can be partially attributed to the decomposition of HCOOH because **1**/G could oxidize HCOOH, as confirmed independently (Figure S12). It was confirmed that HCOOH was the major product even in the methane oxidation reaction for 10 min (entry 22 in Table S1), suggesting that MeOH and HCHO were quickly oxidized in this reaction condition.

https://doi.org/10.1021/jacsau.2c00618
JACS Au 2023, 3, 823−833

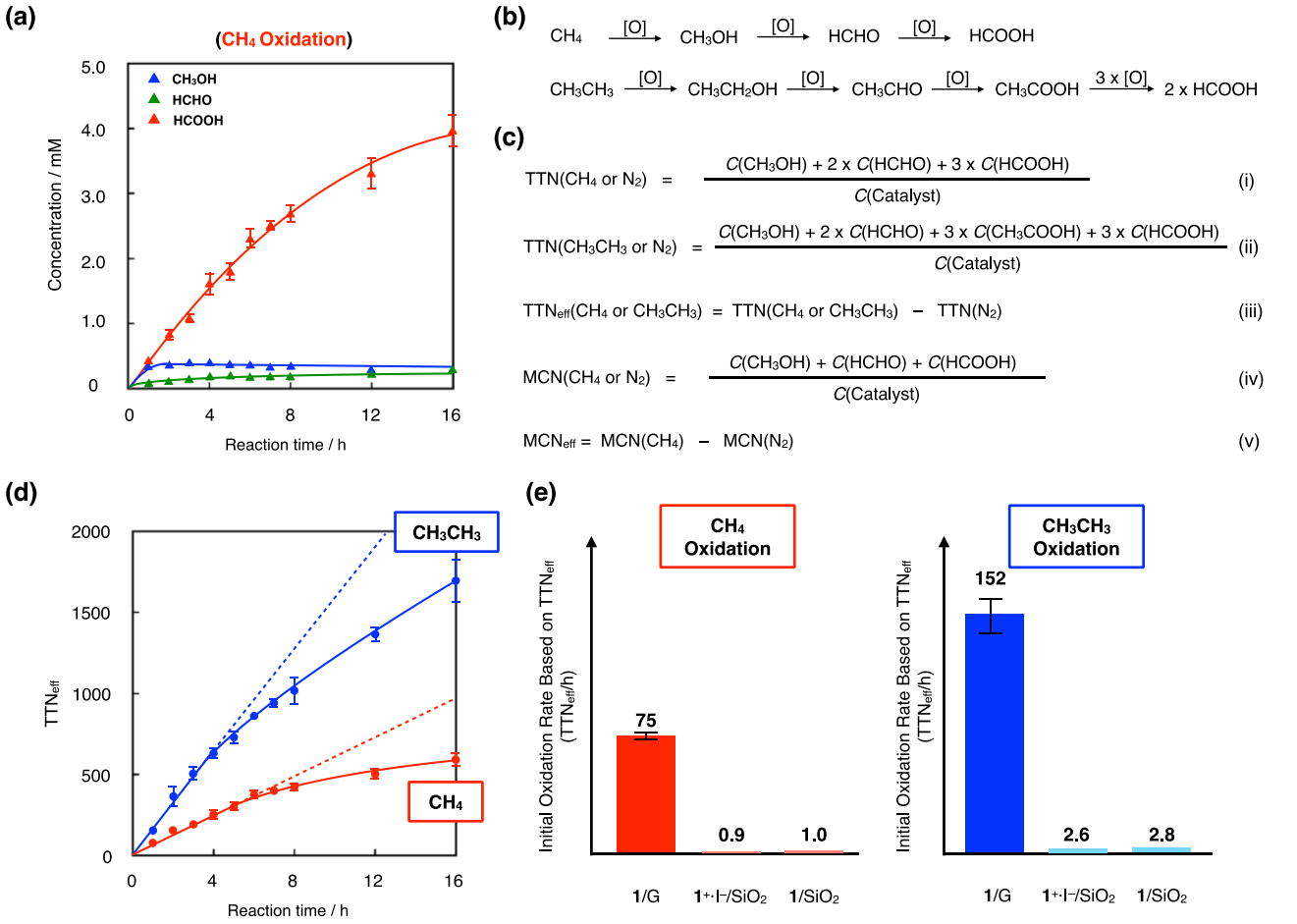

Figure 3. Catalytic activities of the graphite-supported μ-nitrido-bridged iron phthalocyanine dimer (**1**/G) in the oxidation of methane and ethane. (a) Time-dependent change in the concentration of each oxidized product during the oxidation of methane (1.0 MPa) under the catalysis of **1**/G (19 μM as **1**) in an aqueous solution (3.0 mL) containing H_2O_2 (189 mM) and TFA (51 mM) at 60 °C. (b) Stepwise oxidation reactions of methane and ethane. (c) Definitions of the effective total turnover number (TTN_{eff}) of the catalyst in methane and ethane oxidation and effective methane oxidation number (MCN_{eff}). (d) Time-dependent variation in the TTN_{eff} of **1**/G in methane and ethane oxidation. (e) Comparison of the TTN_{eff} of **1**/G in methane and ethane oxidation with those of reference samples ($\mathbf{1}^+\cdot I^-$ and its 1e$^-$-reduced species, **1** loaded on silica supports). Error bars in (a,d,e) indicate the S.D. of three independent reactions conducted using different batches of **1**/G.

As both $\mathbf{1}^+$ [consisting of two Fe(IV) ions] and its 1e$^-$-reduced species **1** [containing one Fe(III) ion and one Fe(IV) ion] are known to act as oxidation catalysts,[22−28] we prepared two different silica-supported catalysts, $\mathbf{1}^+\cdot I^-/SiO_2$ and $\mathbf{1}/SiO_2$, as reference samples.[28] We found that the initial turnover frequency (TTN_{eff}/h) of **1**/G in both methane and ethane oxidation reactions was considerably higher than that of $\mathbf{1}^+\cdot I^-/SiO_2$ and $\mathbf{1}/SiO_2$ (entries 12−15 in Table S1, entries 14−17 in Table S2, and Figure 3e). These results indicate that the significant increase in the oxidizing ability of **1** originates from the interaction between the μ-nitrido-bridged iron phthalocyanine dimer and graphite. The difference in TTN_{eff}s in the methane and ethane oxidation is apparently due to the difference in the C−H bond dissociation energies of the two alkanes (104.9 kcal/mol for methane and 101.4 kcal/mol for ethane). Alkane oxidation by iron porphyrinoids in the presence of H_2O_2 generally competes with the catalase reaction, in which the terminal iron-oxo species (the reactive intermediate generated by the reaction with H_2O_2) oxidizes H_2O_2 to O_2.[38] We found that the catalase reaction by **1**/G was significantly enhanced in comparison with that catalyzed by $\mathbf{1}^+\cdot I^-/SiO_2$ (Figure S13), and almost half of the H_2O_2 (52%) was consumed by this reaction under the same conditions after 8 h. This factor also accounted for the gradual decrease in the reaction rate (Figure 3d). It is considered that O_2 generated during the reaction by catalase reaction did not affect the oxidation reaction because initial O_2 concentration in H_2O did not change the methane oxidation efficiency significantly (entry 21 in Table S1). We also confirmed that the oxidation reaction became slower in the absence of TFA (entry 18 in Table S2), which is considered to facilitate the generation of high-valent terminal iron-oxo species by protonation of the distal oxygen of the Fe−OOH bond of the hydroperoxo species of **1**.[22,23]

Furthermore, we investigated the temperature dependence of the catalytic methane oxidation activity (Figure 4a, entries 1−4). **1**/G exhibited catalytic methane oxidation activity, even at room temperature, and yielded methanol and formaldehyde as the major products. Its TTN_{eff} was found to increase with temperature. In the presence of increased amounts of H_2O_2 (945 mM) at 100 °C, TTN_{eff} and MCN_{eff} reached 600 and 200 h^{-1}, respectively (entry 5 in Figure 4a). Furthermore, a similarly high catalytic methane oxidation activity was realized by irradiating the reaction mixture with a high-pressure Xe lamp equipped with an infrared-blocking mirror module, without using any temperature control apparatus (entry 6 in

https://doi.org/10.1021/jacsau.2c00618
JACS Au 2023, 3, 823−833

(a)

Entry	Catalyst	Reaction Time / h	Reaction Temperature / °C	H_2O_2 / mM	Additional Conditions	[CH_3OH] / mM	[HCHO] / mM	[HCOOH] / mM	TTN(CH_4)	TTN_{eff}	MCN(CH_4)	MCN_{eff}
1	**1**/G	8	25	189	•••	0.32 (0.11)	0.29 (0.16)	0.00 (0.00)	47 (15)	22 (15)	32 (7)	13 (7)
2	**1**/G	8	40	189	•••	0.29 (0.03)	0.39 (0.11)	0.57 (0.04)	145 (19)	118 (19)	65 (9)	44 (9)
3	**1**/G	1	80	189	•••	0.27 (0.00)	0.31 (0.06)	0.81 (0.08)	186 (19)	140 (19)	78 (7)	57 (7)
4	**1**/G	1	100	189	•••	0.37 (0.01)	0.89 (0.07)	2.80 (0.1 7)	591 (29)	549 (29)	228 (10)	208 (10)
5	**1**/G	1	100	945	•••	0.28 (0.03)	0.40 (0.12)	3.81 (0.11)	702 (17)	630 (17)	252 (7)	218 (7)
6	**1**/G	1	No temp. control	189	Photo-irradiation	0.32 (0.02)	1.08 (0.53)	2.55 (0.16)	567 (65)	496 (65)	221 (31)	189 (31)
7	**1**/G	1	20	189	Photo-irradiation	0.13 (0.01)	0.22 (0.06)	0.23 (0.01)	72 (5)	3 (5)	33 (3)	1 (3)

(b)

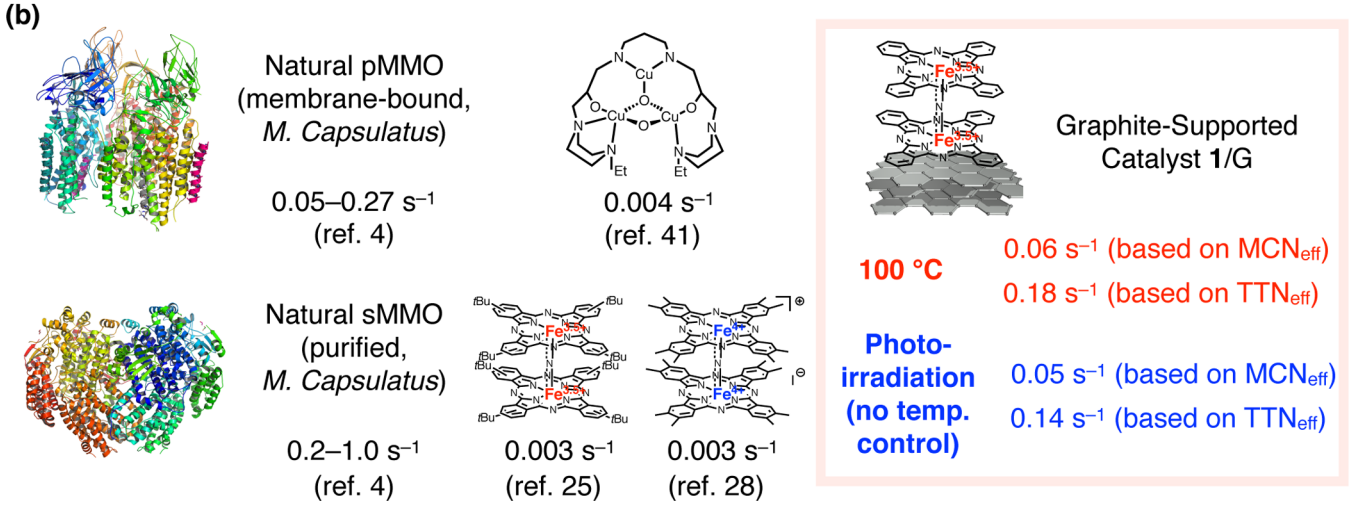

Figure 4. Comparison of catalytic methane oxidation activities of natural and artificial metal-oxo-based molecular catalysts. (a) Summary of the results of methane oxidation. Reactions were performed under 1.0 MPa CH_4 pressure using a graphite-supported catalyst (10 mg, containing 19 μM of **1**) in an aqueous solution (3.0 mL) containing H_2O_2 (189 or 945 mM) and TFA (51 mM) at the given temperature or reaction conditions. The numbers in the parentheses indicate the standard deviation of each value. The results of the reactions in the absence of CH_4 (under N_2; 1.0 MPa) are summarized in Table S3 in the Supporting Information. The details of the reaction conducted under photoirradiation are provided in the Supporting Information. (b) Comparison of the TOFs of MMOs (ref 4) and certain artificial metal-oxo-based molecular catalysts. The TOFs of efficient molecular catalysts reported to date (refs 2528, and 41) were calculated based on their TTNs. The TOFs of **1**/G calculated based on both the effective total turnover number (TTN_{eff}) and the effective methane oxidation number (MCN_{eff}) are shown.

Figure 4a). As TTN_{eff} was much lower when the photo-irradiation-induced reaction was performed at 20 °C with appropriate temperature control (entry 7 in Figure 4a), the high activity under photoirradiation is mainly attributed to light-induced heating owing to the photothermal effect of graphite.[39,40] In fact, the temperature of the reaction mixture increased to ∼70 °C after 1 h of photoirradiation. The realization of high catalytic activity without using any temperature control apparatus is an added advantage of using graphite as a solid support.

Since it was reported that the catalytic oxidation of a phenol derivative by an iron porphyrinoid was significantly accelerated after adsorption onto a graphite surface,[30] we also investigated the catalytic methane oxidation activity of a graphite-supported monomeric iron(II) phthalocyanine (**Fe(II)Pc**/G). As shown in entry 17 in Table S1, the catalytic activity of **Fe(II)Pc**/G (TTN_{eff} = 12 for 1 h of oxidation at 60 °C) was much lower than that of **1**/G (TTN_{eff} = 75 for 1 h of oxidation at 60 °C). Moreover, the methane oxidation reaction by **Fe(II)Pc**/G seemed to proceed mainly via a Fenton-type reaction because it was significantly quenched in the presence of 100 mM Na_2SO_3 (entry 19 in Table S1). Thus, it was demonstrated that the cofacially stacked structure of **1** including Fe−N═Fe moiety is essential for achieving particularly high catalytic methane oxidation activity via the terminal iron-oxo-based reaction mechanism.

Given the high catalytic methane oxidation activity of **1**/G, we compared the initial TOFs (TTN_{eff}/h and MCN_{eff}/h) of **1**/G with those of natural MMOs and other highly active metal oxo-based molecular catalysts (see Figure 4b).[4,25,28,41] Both values indicate that **1**/G exhibits a much higher methane oxidation activity than other efficient biomimetic catalysts reported to date. In order to compare the catalytic activity of **1**/G with that of MMOs, it should be considered that MMOs selectively afford MeOH from methane, whereas the major product by **1**/G was HCOOH. Therefore, it is more

https://doi.org/10.1021/jacsau.2c00618
JACS Au 2023, 3, 823−833

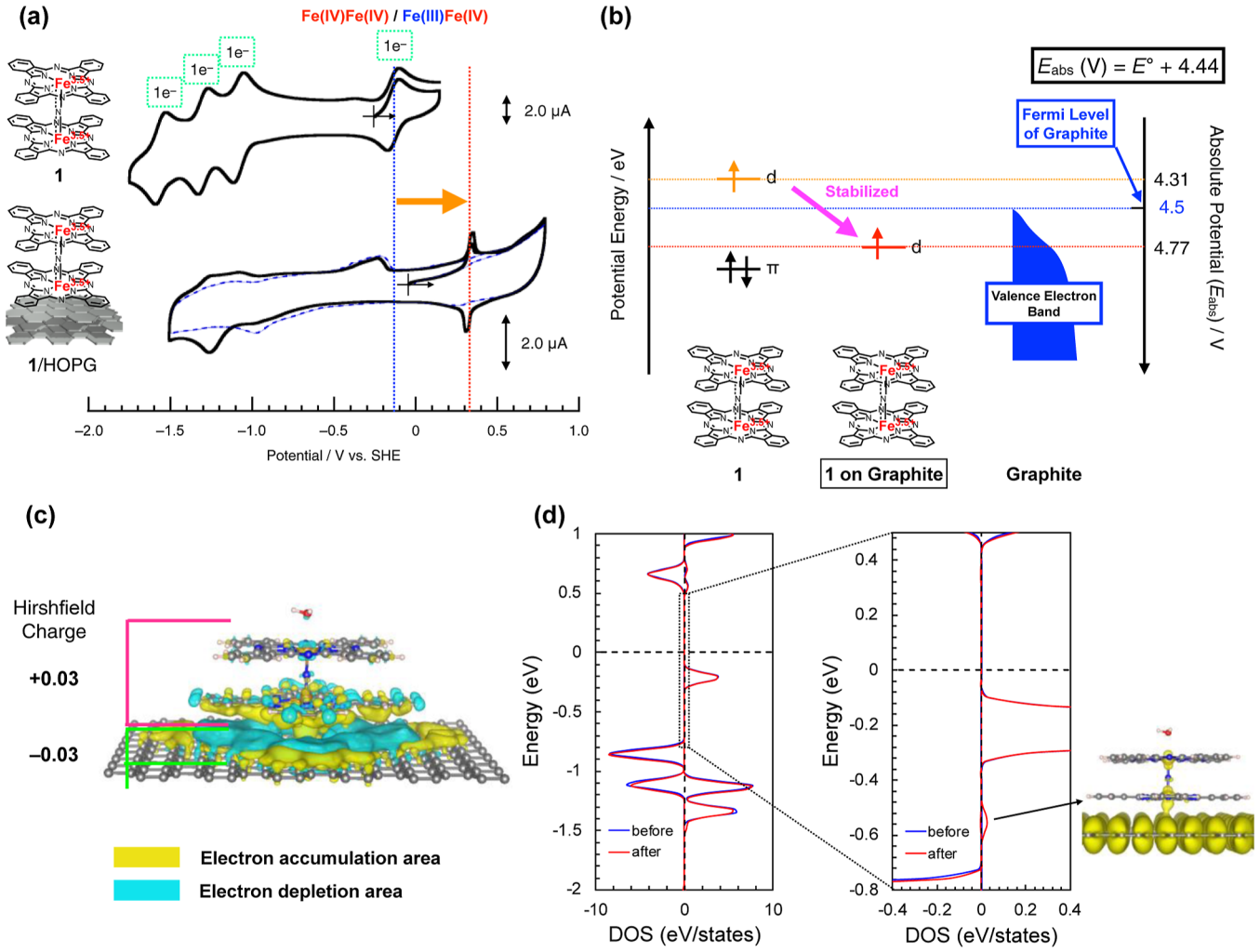

Figure 5. Results of electrochemical measurements and DFT calculations. (a) Comparison of the cyclic voltammograms of **1** in a 400 μM solution (top) and the μ-nitrido-bridged iron phthalocyanine dimer adsorbed on the graphite basal plane in a pyrolytic graphite electrode (bottom, black line). The blue dashed line in the bottom voltammograms represents the results obtained with a bare pyrolytic graphite electrode (without **1**). All voltammograms were recorded in a pyridine solution containing 100 mM $^{n}Bu_4N^{+}PF_6^{-}$ (TBAPF$_6$) at 20 °C at a scan rate of 0.1 V/s. (b) Comparison of the SOMO energy levels for the μ-nitrido-bridged iron phthalocyanine dimer, **1** (neutral species, in a pyridine solution), and for **1** adsorbed on the graphite surface (**1**/HOPG) with the Fermi level of graphite obtained based on the absolute redox potentials calculated from the cyclic voltammograms. (c) Charge density difference for the adsorption of **1** on the surface of graphene. Electron accumulation and depletion are represented by yellow and blue areas, respectively (isovalue is set to 5.0×10^{-4} Å^{-3}). (d) Comparison of spin-up (positive values) and spin-down (negative values) density of states projected on the Fe atom closer to graphene before (blue) and after (red) adsorption. The Fermi level is set to 0 eV. A close-up view of the Fermi level is also shown. A new state is generated at $E = -0.58$ eV upon adsorption. The charge density isosurface corresponding to the state is shown in the inset (isovalue is set to 3.0×10^{-4} Å^{-3}).

appropriate to use MCN$_{eff}$ instead of TTN$_{eff}$ for this comparison because MCN$_{eff}$ directly reflects the number of C−H activation of methane. Taking that the TOF of **1**/G based on MCN$_{eff}$ reached 200 h^{-1} at 100 °C (0.06 s^{-1}), **1**/G showed comparable methane oxidation activity to that of membrane-bound pMMO (*Methylococcus capsulatus*), whose TOF was reported to be 0.05−0.27 s^{-1} (Figure 4b), at least in terms of C−H activation of methane.[4]

One important point to be considered here is that the catalytic activity of pMMO was measured at ambient temperature using aqueous solutions saturated with CH$_4$. In general, natural enzymes are deactivated at higher temperature around 100 °C, whereas **1**/G showed high catalytic activity at 100 °C because of its high thermal stability. This is also a merit of using an artificial catalyst. On the other hand, MeOH selectivity of CH$_4$ oxidation by **1**/G was much lower than that by pMMO. In order to improve the MeOH selectivity of **1**/G, it is considered that appropriate chemical modification around the reaction center of **1**/G would be effective.

Investigation of the Electronic State of the Catalyst on Graphite

To clarify the reasons for the high catalytic activity of **1**/G, the electronic state of the catalyst on graphite was investigated by cyclic voltammetry using **1** adsorbed onto the basal plane of graphite in a pyrolytic graphite electrode. A sufficient amount of the catalyst was adsorbed onto the electrode surface as in the case with the HOPG modification by simply dipping the electrode in a pyridine solution of $\mathbf{1}^{+}\cdot I^{-}$, implying that this catalyst molecule is prone to be adsorbed on the π-surface of graphite. As shown in Figure 5a, the change in the voltammogram of the catalytic center suggests a dramatic change in the electronic structure of the catalyst, after

https://doi.org/10.1021/jacsau.2c00618
JACS Au 2023, 3, 823−833

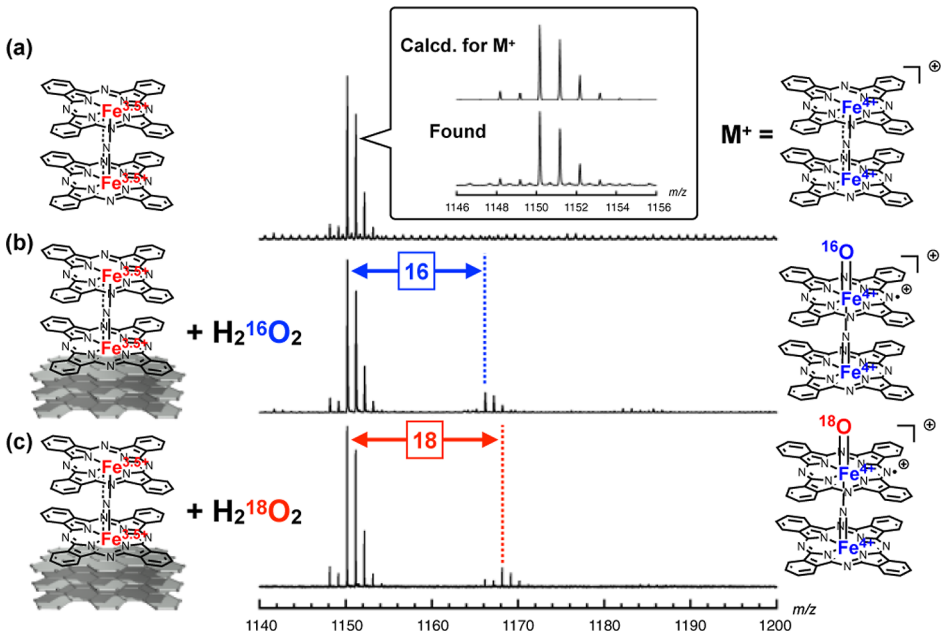

Figure 6. MALDI-TOF MS spectra of (a) **1**/HOPG, (b) $H_2{}^{16}O_2$-treated **1**/HOPG, and (c) $H_2{}^{18}O_2$-treated **1**/HOPG.

adsorption onto the electrode surface. The graphite electrodes treated with both **1** and $\mathbf{1}^{+}\cdot I^{-}$ yielded almost identical voltammograms (Figure S14), suggesting that $\mathbf{1}^{+}\cdot I^{-}$ was reduced by one electron to neutral species **1** during its adsorption onto the graphite surface. In particular, the reversible 1e^{-}-redox wave assignable to Fe(IV)−N═Fe(IV)/Fe(III)−N═Fe(IV) showed a significant positive shift ($\Delta E^{\circ\prime}$ = 0.463 V).[42] We confirmed that the difference in the type of counteranion present in the supporting electrolyte and the coordinating solvent associated with the iron ions in **1** did not significantly affect the degree of positive shift (Figure S15 and Table S4). Therefore, we inferred that the positive shift of the redox potential implies that the singly occupied molecular orbital (SOMO) level of **1** decreased significantly after its adsorption onto the support. The absolute electrode potential (E_{abs}) calculated from the redox potentials confirmed that the SOMO level of adsorbed **1** (4.77 V) was lower than that of graphite (~4.5 eV), as shown in Figure 5b.[43,44]

The positive shift in the 1e^{-}-oxidation waves in the cyclic voltammogram could suggest charge transfer from **1** to graphite because the iron center of **1** became more electron deficient after adsorption. In fact, for monomeric iron(II) phthalocyanine (**Fe(II)Pc**) on graphene, partial charge transfer from iron(II) phthalocyanine to graphite has been predicted by theoretical calculations.[45] Therefore, density functional theory (DFT) calculations of the stacked conjugate of graphene and **1** with coordinating H_2O were conducted using VASP software. The calculations indicated slight charge transfer from **1** to the graphene surface, as in the case of **Fe(II)Pc**. Interestingly, most of the transferred charges were distributed between the graphene and the adsorbed iron(II) phthalocyanine, whereas the non-adsorbed iron(II) phthalocyanine unit of **1**, including the coordinated H_2O, was almost free from the transferred charge (Figure 5c). Moreover, the SOMO of **1** interacted in a bonding manner with the π-orbital of graphene to produce a new orbital with lower energy, which is consistent with the lowered SOMO level deduced based on the electrochemical measurement results (Figure 5d).

To confirm the effect of stacking between **Fe(II)Pc** and graphite on the electrochemical properties, cyclic voltammetry was performed on a pyrolytic graphite electrode with **Fe(II)Pc** adsorbed on the basal plane of graphite. The oxidation potential corresponding to Fe(III)/Fe(II) exhibited a significant positive shift (Figure S16), although the oxidation process was irreversible. This indicates the instability of the stacked conjugate of positively charged monomeric iron phthalocyanine units on the graphite surface, which is in clear contrast to the reversible redox wave observed for **1** adsorbed onto the graphite surface (Figure 5a). Thus, the cofacially stacked structure of **1** seemed to contribute to stable adhesion onto the graphite surface.

We also checked the cyclic voltammogram of μ-carbido-bridged iron phthalocyanine dimer **2** (structure shown on page S28) having a cofacially stacked iron phthalocyanine structure similar to **1**. In this case, although a reversible 1e^{-} redox wave was observed, assignable to the oxidation of **2** (shown in Figure S17), an apparent positive shift in the redox wave, comparable to **1**, was not observed. The most conspicuous structural difference between **1** and **2** is the difference in the conjugated structure along the Fe−X−Fe (X = N or C) core, where **1** has S = 1/2 spin and **2** has no isolated spin (S = 0).[46−48] DFT calculations suggested that the SOMO of **1** interacted in a bonding manner with the π-orbital of graphene to produce a new orbital with a lower energy (Figure 5d). Therefore, the efficient conjugation of the SOMO spin of **1** with the graphite orbital might be the key to elucidating the apparent SOMO stabilization.

Proposed Mechanism for Increased Catalytic Methane Oxidation Activity of μ-Nitrido-Bridged Iron Phthalocyanine Dimer on Graphite

The reactive species in alkane oxidation, catalyzed by a μ-nitrido-bridged iron phthalocyanine dimer, is considered to be a high-valent terminal iron-oxo species, generated by the reaction of the catalyst with H_2O_2 (Figure 1b).[22,24] We confirmed the generation of the terminal iron-oxo species onto the graphite surface by high-resolution MALDI-TOF mass

https://doi.org/10.1021/jacsau.2c00618
JACS Au 2023, 3, 823−833

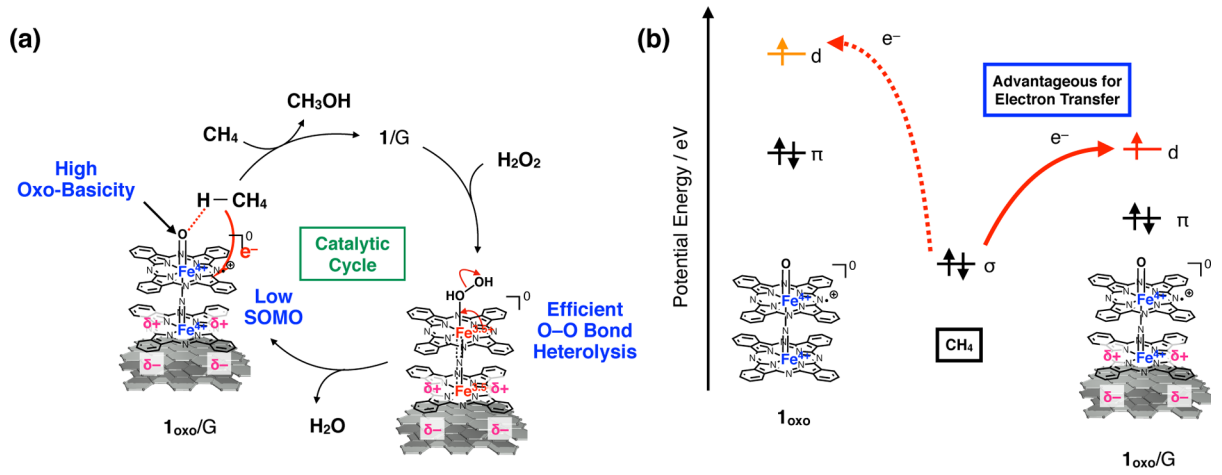

Figure 7. Possible elucidation of the high catalytic activity of **1**/G. (a) Proposed reactions involved in the high methane conversion under the catalysis of **1**/G based on the reaction of $\mathbf{1}_{oxo}$. (b) A lower SOMO level of the high-valent terminal iron-oxo species of the μ-nitrido-bridged iron phthalocyanine dimer could be achieved through its interaction with graphite. This is likely to favor the PCET from methane.

spectroscopy as shown in Figure 6. **1** on **1**/G was observed as $\mathbf{1}^+$, presumably because it was oxidized by $1e^-$ during the MALDI measurement. The short-term treatment of **1**/HOPG with $H_2{}^{16}O_2$ or $H_2{}^{18}O_2$ resulted in the generation of the $[\mathbf{1} + O]^+$ species, which corresponds to the calculated mass number of the high-valent terminal iron-oxo species, $\mathbf{1}_{oxo}$ generated on HOPG. It was confirmed that the peaks corresponding to the reactive oxo species completely disappeared after treatment with tetrahydrofuran. It should also be noted that loading too much matrix layer on **1**/HOPG treated with H_2O_2 did not give the peaks corresponding to the oxo species. Therefore, we concluded that $\mathbf{1}_{oxo}$ was successfully observed.

Based on the results obtained, we propose a possible mechanism for the high methane conversion in the presence of **1**/G, based on the reaction of $\mathbf{1}_{oxo}$, as illustrated in Figure 7a.[22−25] The reaction of **1**/G with H_2O_2 resulted in the formation of H_2O_2 adduct **1**(**HOOH**)/G. Heterolytic cleavage of the O−O bond in **1**(**HOOH**) produces high-valent terminal iron-oxo species $\mathbf{1}_{oxo}$/G, which acts as a reactive intermediate for methane oxidation. Based on knowledge of the PCET mechanism, the key factors for achieving efficient methane oxidation are high oxo-basicity, for efficient H atom abstraction, and a more positive redox potential of the catalyst, for achieving electron transfer from methane.[8−19] As the electronic structure of $\mathbf{1}_{oxo}$ is similar to that of **1**, in which a SOMO with $S = 1/2$ spin is distributed mainly over the O═Fe−N═Fe center,[22,47] it can be assumed that the SOMO level of $\mathbf{1}_{oxo}$ was stabilized in a manner similar to that observed for **1** (Figure 7b). This is likely to be beneficial for achieving a more positive redox potential for $\mathbf{1}_{oxo}$. On the other hand, partial charge transfer from the catalyst to graphite seems to be unfavorable for both electron donation from the iron phthalocyanine of **1**(**HOOH**)/G, to facilitate the heterolytic cleavage of O−O bonds, and the high oxo-basicity of $\mathbf{1}_{oxo}$. In the case of monomeric iron tetraphenyl porphyrin, it is known that electron-withdrawing substituents introduced on the *meso*-phenyl groups decrease the formation rate of the high-valent terminal iron-oxo species.[49] However, in the case of **1**/G, owing to the cofacially stacked structure, positive charges were localized mainly on the phthalocyanine unit directly stacked on graphite as in the case of the structure shown in Figure 5c and did not significantly affect the oxo-basicity and formation rate of the oxo species (Figure 7a). Overall, **1**/G showed high catalytic activity for methane oxidation.

CONCLUSIONS

We demonstrated that a graphite-supported molecular catalyst having a cofacially stacked structure exhibits high activity for methane and ethane oxidation. This catalyst consists of a μ-nitrido-bridged iron phthalocyanine dimer, closely stacked onto a graphite support. The catalytic methane oxidation activity of the μ-nitrido-bridged iron phthalocyanine dimer increased dramatically after its adsorption onto a graphite surface, to a level comparable to a membrane-bound pMMO, with regard to the turnover efficiency for the C−H activation of methane. In addition, photoirradiation of the catalyst led to high catalytic methane oxidation activity without requiring any temperature control apparatus owing to the photothermal effect of the graphite support. On the other hand, monomeric iron(II) phthalocyanine adsorbed on the graphite surface exhibited much lower catalytic activity than the cofacially stacked complex, indicating the superiority of the adsorption of the cofacially stacked complex for achieving higher methane oxidation activity.

Spectroscopic and electrochemical analyses of the catalyst, in combination with DFT calculations, suggested that a lower SOMO level of the high-valent terminal iron-oxo species, beneficial for PCET with methane, could be achieved because of the interaction of the SOMO of the catalyst molecule with the π-orbital of graphite. Furthermore, it was demonstrated that the cofacially stacked structure of the catalyst could contribute to the prevention of a decrease in the formation rate of the reactive terminal iron-oxo species, as well as the significant decrease in the oxo-basicity. We confirmed that the cofacially stacked structure ensured the stability of the catalytic center during oxidation. Thus, to achieve high catalytic methane oxidation activity, the close stacking of a metal complex having a cofacially stacked structure and graphite must be significantly different from that between a monomeric metal complex and graphite. This graphite-supported cofacially stacked complex can be used to fabricate catalyst-modified carbon electrodes. Exploring the interaction of a solid support, such as graphite, with a metal complex having a cofacially stacked structure could prove to be a unique strategy for

https://doi.org/10.1021/jacsau.2c00618
JACS Au 2023, 3, 823−833

overcoming the limitations of molecular catalysts, not only in methane oxidation but also in a wide variety of other reactions.

METHODS

General Information

All the reagents and solvents were purchased at the highest commercial quality available and used as received without further purification, unless otherwise stated. A monocationic μ-nitrido-bridged iron phthalocyanine dimer $\mathbf{1}^{+}\cdot I^{-}$ was prepared according to our previously reported procedure.[32] Its $1e^{-}$-reduced species **1** was prepared by a slight modification of the procedure reported by Ercolani et al., undertaken in a glovebox purged with Ar, as described in the Supporting Information.[31] MALDI-TOF mass spectrometry was performed using a Bruker Daltonics UltrafleXtream spectrometer. Elemental analyses were performed on a Yanaco MT-6 analyzer.

Preparation of Solid-Supported Catalysts

A monocationic μ-nitrido-bridged iron phthalocyanine dimer $\mathbf{1}^{+}\cdot I^{-}$ (7.4 mg, 5.3 μmol as a pyridine adduct) was dissolved in pyridine (8 mL). After mixing with a suspension of graphite (0.93 g, powder, Wako Chemical Corp.) in pyridine (12 mL), the mixture was sonicated for 1 h. The resulting suspension was stirred for 24 h at 80 °C. During the stirring, the color of the solution phase almost disappeared as shown in Figure S1. After the solvent was filtered off, the solid was washed with pyridine (50 mL × 2) and CH_2Cl_2 (50 mL × 3) in succession and dried under reduced pressure (~1 mmHg) at 80 °C for 7 h.

The obtained solid was suspended in H_2O (30 mL) containing 3.0 mL of TFA. After the resulting suspension was sonicated for 1 h, the solid was filtered and washed with H_2O until the pH of the filtrate became neutral. This washing procedure was repeated three times. Finally, the obtained solid was dried under reduced pressure (~1 mmHg) to obtain the solid-supported catalyst **1**/G (0.92 g). A graphite-supported catalyst of a monomeric iron(II) phthalocyanine (**Fe(II)Pc**/G) was prepared in a similar manner. The silica-supported catalysts ($\mathbf{1}^{+}\cdot I^{-}/SiO_2$ and $\mathbf{1}/SiO_2$) were prepared in the same manner. Silica gel was purchased from Merck (Silica gel 60, 0.040−0.063 mm) and used after washing with CH_2Cl_2 and H_2O, followed by drying under reduced pressure at 80 °C for 24 h.

Preparation of HOPG Substrate on which 1 Was Adsorbed (1/HOPG)

A freshly cleaved HOPG [7 × 7 × 0.5 mm, Alliance Biosystems, SPI-1(ZYA) grade] was soaked in a solution of a monocationic μ-nitrido-bridged iron phthalocyanine dimer $\mathbf{1}^{+}\cdot I^{-}$ pyridine [9.0 mg (6.4 μmol)] in pyridine (30 mL) for 8 h. After washing twice with pyridine, the HOPG was dried under vacuum (~1 mmHg) at 80 °C for 16 h to prepare a HOPG on which **1** was adsorbed (**1**/HOPG). This HOPG substrate was used for NEXAFS, XPS, and MALDI-TOF MS measurements. A HOPG treated with the neutral form of a μ-nitrido-bridged iron phthalocyanine dimer was prepared in the same manner.

Oxidation Reactions

Methane or ethane oxidation was performed in a stainless steel autoclave with a glass tube. A mixture of a solid-supported catalyst [10 mg, 19 μM as **1** or $\mathbf{1}^{+}$, or **Fe(II)Pc**], TFA (12 μL, 51 mM), and 35% H_2O_2 aq (50 μL, 189 mM) in H_2O (3.0 mL) was heated at 60 °C under a methane (or ethane) atmosphere of 1.0 MPa for 1−16 h. After the reaction mixture was filtered through a disposable membrane filter (ADVANTEC, DISMIC-13CP), the resulting filtrate was mixed with an appropriate amount of isovaleric acid solution (100 mM) and analyzed by GC−MS [system: Shimadzu GCMS-QP2020, detection: EI, column: Agilent DB-WAX UI, external standard: isovaleric acid (5 mM), temperature conditions: initial: 50 °C—hold (1 min)—raise to 220 °C (10 °C/min)— hold (5 min)]. The yields of methanol, ethanol, acetaldehyde, acetic acid, and formic acid were determined based on the results of GC−MS. Although alcohols and aldehydes generated in situ formed hemiacetals in an acidic reaction condition as demonstrated in the NMR measurements (Figures S8 and S9), the hemiacetals seemed to dissociate under GC−MS conditions.

The yield of formaldehyde was determined using the method reported by Ho and Yu.[50] Typically, 25 μL of the filtrate obtained from the reaction mixture was diluted with 50 mL of H_2O, followed by the addition of an aqueous solution (469 μM) of PFBOA·HCl (3.0 mL). The resulting mixture was stirred for 2 h. Then, sulfuric acid (1 + 1) (0.8 mL), NaCl (20 g), and hexane (5.0 mL) were added, and the mixture was stirred vigorously for 5 min. The separated organic layer was dried over anhydrous Na_2SO_4. A mixture of the resulting solution (1.0 mL) and a 1.0 mM 1-chlorodecane/hexane solution (10.1 μL) was analyzed by GC−MS [Agilent 7890A equipped with JEOL JMS-T100GCV, detection: EI, column: Agilent DB-WAX UI, external standard: 1-chlorodecane (10 μM), temperature conditions: initial: 70 °C—hold (10 min)—raise to 150 °C (10 °C/min)—raise to 240 °C (30 °C/min)—hold (3 min)].

The blank experiments were performed under a N_2 atmosphere just before the methane or ethane oxidation to confirm the absence of contaminants. The oxidized products observed in the absence of methane or ethane were presumably derived from the adsorbed organic solvents on the solid supports (SiO_2 or graphite). It was also found that the errors of the TTN_{eff}s of methane or ethane oxidation by the solid-supported catalysts were at most ±5% for methane oxidation and ±8% for ethane oxidation.

As for the methane oxidation using O_2-saturated H_2O, a mixture containing **1**/G (10 mg, 19 μM as **1**), TFA (12 μL, 51 mM), and 35% H_2O_2 aq (50 μL, 189 mM) in O_2 saturated H_2O (3.0 mL) was heated at 60 °C for 6 h under a CH_4 atmosphere of 1.0 MPa in a stainless steel autoclave with a glass tube.

ASSOCIATED CONTENT

Supporting Information

The Supporting Information is available free of charge at https://pubs.acs.org/doi/10.1021/jacsau.2c00618.

Detailed experimental procedures for the synthesis of a neutral μ-nitrido-bridged iron phthalocyanine dimer (**1**), XPS measurements, NEXAFS measurements, ^{1}H-NMR measurement of the reaction mixtures of light alkane oxidation, oxidation of ^{13}C-labeled CH_4, GC analysis of gaseous phase in the absence of substrate, oxidation of HCOOH, evaluation of catalase activities of solid-supported catalysts, photoirradiation reactions, cyclic voltammogram measurements, DFT calculation, and MALDI-TOF measurement of **1**/HOPG and H_2O_2-treated **1**/HOPG (PDF)

AUTHOR INFORMATION

Corresponding Authors

Yasuyuki Yamada − *Department of Chemistry, Graduate School of Science, Nagoya University, Nagoya 464-8602, Japan; Research Center for Materials Science, Nagoya University, Nagoya 464-8602, Japan;* orcid.org/0000-0002-3197-4612; Email: yamada.yasuyuki.i6@f.mail.nagoya-u.ac.jp

Kentaro Tanaka − *Department of Chemistry, Graduate School of Science, Nagoya University, Nagoya 464-8602, Japan;* orcid.org/0000-0002-6395-4536; Email: kentaro@chem.nagoya-u.ac.jp

Authors

Kentaro Morita − *Department of Chemistry, Graduate School of Science, Nagoya University, Nagoya 464-8602, Japan*

Takuya Sugiura − *Department of Chemistry, Graduate School of Science, Nagoya University, Nagoya 464-8602, Japan*

https://doi.org/10.1021/jacsau.2c00618
JACS Au 2023, 3, 823−833

Yuka Toyoda − *Department of Chemistry, Graduate School of Science, Nagoya University, Nagoya 464-8602, Japan*
Nozomi Mihara − *Department of Chemistry, Graduate School of Science, Nagoya University, Nagoya 464-8602, Japan*
Masanari Nagasaka − *Institute for Molecular Science, Okazaki 444-8585, Japan;* orcid.org/0000-0002-6249-6553
Hikaru Takaya − *Institute for Molecular Science, Okazaki 444-8585, Japan*
Kiyohisa Tanaka − *Institute for Molecular Science, Okazaki 444-8585, Japan*
Takanori Koitaya − *Institute for Molecular Science, Okazaki 444-8585, Japan;* orcid.org/0000-0001-8793-1518
Naoki Nakatani − *Department of Chemistry, Graduate School of Science, Tokyo Metropolitan University, Hachioji 192-0397 Tokyo, Japan;* orcid.org/0000-0002-9100-137X
Hiroko Ariga-Miwa − *Institute for Catalysis, Hokkaido University, Sapporo 001-0021 Hokkaido, Japan*
Satoru Takakusagi − *Institute for Catalysis, Hokkaido University, Sapporo 001-0021 Hokkaido, Japan;* orcid.org/0000-0002-4095-172X
Yutaka Hitomi − *Department of Molecular Chemistry and Biochemistry, Graduate School of Science and Engineering, Doshisha University, Kyotanabe 610-0321 Kyoto, Japan;* orcid.org/0000-0002-2448-296X
Toshiji Kudo − *Daltonics Division, Bruker Japan K.K., Yokohama-shi 221-0022 Kanagawa, Japan*
Yuta Tsuji − *Institute for Materials Chemistry and Engineering and IRCCS, Kyushu University, Fukuoka 819-0385, Japan;* Present Address: Faculty of Engineering Sciences, Kyushu University, Kasuga, Fukuoka 816-8580, Japan; orcid.org/0000-0003-4224-4532
Kazunari Yoshizawa − *Institute for Materials Chemistry and Engineering and IRCCS, Kyushu University, Fukuoka 819-0385, Japan;* orcid.org/0000-0002-6279-9722

Complete contact information is available at: https://pubs.acs.org/10.1021/jacsau.2c00618

Author Contributions

CRediT: **Yasuyuki Yamada** conceptualization, data curation, formal analysis, funding acquisition, investigation, methodology, project administration, writing-original draft, writing-review & editing; **Kentaro Morita** data curation; **Takuya Sugiura** data curation; **Yuka Toyoda** data curation, formal analysis; **Nozomi Mihara** data curation, formal analysis; **Masanari Nagasaka** data curation, formal analysis; **Hikaru Takaya** data curation, formal analysis; **Kiyohisa Tanaka** data curation, formal analysis; **Takanori Koitaya** data curation, formal analysis; **Naoki Nakatani** data curation, investigation; **Hiroko Ariga-Miwa** data curation, formal analysis; **Satoru Takakusagi** data curation, formal analysis; **Yutaka Hitomi** data curation, formal analysis, methodology, writing-review & editing; **Toshiji Kudo** data curation, formal analysis; **Yuta Tsuji** data curation, formal analysis; **Kazunari Yoshizawa** data curation, formal analysis; **Kentaro Tanaka** data curation, funding acquisition, investigation, project admission, writing-review & editing.

Notes

The authors declare no competing financial interest.

ACKNOWLEDGMENTS

This work was financially supported by JST PRESTO (14J04135), a JSPS KAKENHI Grant-in-Aid for challenging Exploratory Research (16K13961 and 22K19045) and a Grant-in-Aid for Scientific Research (B) (19H02787 and 22H02156) awarded to Y.Y., and a JSPS KAKENHI Grant-in-Aid for Scientific Research (A) (15H02167 and 19H00902) and a Grant-in-Aid for Scientific Research (B) (22H02094) awarded to KeT. Y.Y. thanks the financial support by Tatematsu Foundation, Iwatani Naoji Foundation, and Toyoaki Scholarship Foundation. This study was also supported by the Cooperative Research Program of Institute for Catalysis, Hokkaido University. (Proposals 18B1013, 21B1006, and 22DS0073.) We thank Prof. J. Yoshinobu and Prof. K. Asakura for the fruitful discussion with them.

REFERENCES

(1) Schwach, P.; Pan, X.; Bao, X. Direct conversion of methane to value-added chemicals over heterogeneous catalysts: challenges and prospect. *Chem. Rev.* **2017**, *117*, 8497−8520.
(2) Ravi, M.; Ranocchiari, M.; van Bokhoven, J. A. The direct catalytic oxidation of methane to methanol−a critical assessment. *Angew. Chem., Int. Ed.* **2017**, *56*, 16464−16483.
(3) Tinberg, C. E.; Lippard, S. J. Dioxygen activation in soluble methane monooxygenase. *Acc. Chem. Res.* **2011**, *44*, 280−288.
(4) Sirajuddin, S.; Rosenzweig, A. C. Enzymatic oxidation of methane. *Biochemistry* **2015**, *54*, 2283−2294.
(5) Wang, V. C. -C.; Maji, S.; Chen, P. P. -Y.; Lee, H. K.; Yu, S. S. -F.; Chan, S. I. Alkane oxidation: methanemonooxyganases, related enzymes, and their biomimetics. *Chem. Rev.* **2017**, *117*, 8574−8621.
(6) McDonald, A. R.; Que, L., Jr. High-valent nonheme iron-oxo complexes: synthesis, structure, and spectroscopy. *Coord. Chem. Rev.* **2013**, *257*, 414−428.
(7) Guo, M.; Corona, T.; Ray, K.; Nam, W. Heme and nonheme high-valent iron and manganese oxo cores in biological and abiological oxidation reactions. *ACS Cent. Sci.* **2019**, *5*, 13−28.
(8) Weinberg, D. R.; Gagliardi, C. J.; Hull, J. F.; Murphy, C. F.; Kent, C. A.; Westlake, B. C.; Paul, A.; Ess, D. H.; McCafferty, D. G.; Meyer, T. J. Proton-coupled electron transfer. *Chem. Rev.* **2012**, *112*, 4016−4093.
(9) Hammes-Schiffer, S. Proton-coupled electron transfer: moving together and charging forward. *J. Am. Chem. Soc.* **2015**, *137*, 8860−8871.
(10) Klein, J. E. M. N.; Knizia, G. cPCET versus HAT: a direct theoretical method for distinguishing X−H bond−Activation mechanism. *Angew. Chem., Int. Ed.* **2018**, *57*, 11913−11917.
(11) Sastri, C. V.; Lee, J.; Oh, K.; Lee, Y. J.; Lee, T. A.; Jackson, K.; Ray, H.; Hirao, W.; Shin, J. A.; Halfen, J.; Kim, L., Jr.; Que, S.; Shaik, W.; Nam, W. Axial ligand tuning of a nonheme iron(IV)-oxo unit for hydrogen atom abstraction. *Proc. Natl. Acad. Sci. U.S.A.* **2007**, *104*, 19181−19186.
(12) Jeong, Y. J.; Kang, Y.; Han, Y. -M.; Lee, H.; Kotani, S.; Fukuzumi, W.; Nam, W. Hydrogen atom abstraction and hydride transfer reactions by iron(IV)-oxo porphyrin. *Angew. Chem., Int. Ed.* **2008**, *120*, 7431−7434.
(13) Tahsini, L.; Bagherzadeh, M.; Nam, W.; de Visser, S. P. Functional difference of substrate hydroxylation by high-valent iron(IV)-oxo model of cytochrome P450. *Inorg. Chem.* **2009**, *48*, 6661−6669.
(14) Usharani, D.; Lacy, D. C.; Borovik, A. S.; Shaik, S. Dichotomous hydrogen atom transfer vs proton-coupled electron transfer during activation of X−H bonds (X = C, N, O) by nonheme iron-oxo complexes of variable basicity. *J. Am. Chem. Soc.* **2013**, *135*, 17090−17104.
(15) Pattanayak, S.; Jasniewski, A. J.; Rana, A.; Draksharapu, A.; Singh, K. K.; Weitz, A.; Hendrich, M.; Que, L., Jr.; Dey, A.; Sen Gupta, S. S. Spectroscopic and reactivity comparisons of a pair of bTAML complexes with Fe^{V}=O and Fe^{IV}=O units. *Inorg. Chem.* **2017**, *56*, 6352−6361.
(16) Borovik, A. S. Role of metal-oxo complexes in the cleavage of C−H bonds. *Chem. Soc. Rev.* **2011**, *40*, 1870−1874.

(17) Fujii, H. Effects of the electron-withdrawing power of substituents on the electronic structure and reactivity in oxoiron(IV) porphyrin π-cation radical complexes. *J. Am. Chem. Soc.* **1993**, *115*, 4641−4648.
(18) Green, M. T.; Dawson, J. H.; Gray, H. B. Oxoiron(IV) in chloroperoxidase compound II is basic: implications for P450 chemistry. *Science* **2004**, *304*, 1653−1656.
(19) Comba, P.; Löhr, A. -M.; Pfaff, F.; Ray, K. Redox potential of high-valent iron-, cobalt, and nickel-oxo complexes: evidence for exchange enhanced reactivity. *Isr. J. Chem.* **2020**, *60*, 957−962.
(20) Sorokin, A. B. Phthalocaynine metal complexes in catalysis. *Chem. Rev.* **2013**, *113*, 8152−8191.
(21) Sorokin, A. B. From mononuclear iron phthalocyanines in catalysis to μ-nitrido diiron complexes and beyond. *Catal. Today* **2021**, *373*, 38−58.
(22) Afanasiev, P.; Sorokin, A. B. μ−Nitrido diiron macrocyclic platform: particular structure for particular catalysis. *Acc. Chem. Res.* **2016**, *49*, 583−593.
(23) Sorokin, A. B.; Kudrik, E. V.; Bouchu, D. Bio-inspired oxidation of methane in water catalyzed by *N*-bridged diiron phthalocyanine complex. *Chem. Commun.* **2008**, 2562−2564.
(24) Kudrik, E. V.; Afanasiev, P.; Alvarez, L. X.; Dubourdeaux, P.; Clémancey, M.; Latour, J.-M.; Blondin, G.; Bouchu, D.; Albrieux, F.; Nefedov, S. E.; Sorokin, A. B. An *N*-bridged high-valent diiron-oxo species on a porphyrin platform that can oxidize methane. *Nat. Chem.* **2012**, *4*, 1024−1029.
(25) İşci, Ü.; Faponle, A. S.; Afanasiev, P.; Albrieux, F.; Briois, V.; Ahsen, V.; Dumoulin, F.; Sorokin, A. B.; de Visser, S. P. Site-selective formation of an iron(iv)-oxo species at the more electron-rich iron atom of heteroleptic μ-nitrido diiron phthalocyanines. *Chem. Sci.* **2015**, *6*, 5063−5075.
(26) Yamada, Y.; Morita, K.; Mihara, N.; Igawa, K.; Tomooka, K.; Tanaka, K. Catalytic methane oxidation by a supramolecular conjugate based on a μ-nitrido-bridged iron porphyrinoid dimer. *New J. Chem.* **2019**, *43*, 11477−11482.
(27) Mihara, N.; Yamada, Y.; Takaya, H.; Kitagawa, Y.; Igawa, K.; Tomooka, K.; Fujii, H.; Tanaka, K. Site-selective supramolecular complexation activates catalytic ethane oxidation by a nitride-bridged iron porphyrinoid dimer. *Chem.—Eur. J.* **2019**, *25*, 3369−3375.
(28) Yamada, Y.; Kura, J.; Toyoda, Y.; Tanaka, K. High catalytic methane oxidation activity of monocationic μ-nitrido-bridged iron phthalocyanine dimer with sixteen methyl groups. *Dalton Trans.* **2021**, *50*, 6718−6724.
(29) Cui, X.; Li, H.; Wang, Y.; Hu, Y.; Hua, L.; Li, H.; Han, X.; Liu, Q.; Yang, F.; He, L.; Chen, X.; Li, Q.; Xiao, J.; Deng, D.; Bao, X. Room-temperature methane conversion by graphene-confined single iron atoms. *Chem* **2018**, *4*, 1902−1910.
(30) Xue, T.; Jiang, S.; Qu, Y.; Su, Q.; Cheng, R.; Dubin, S.; Chiu, C. -Y.; Kaner, R.; Huang, Y.; Duan, X. Graphene−supported hemin as a highly active biomimetic oxidation catalyst. *Angew. Chem., Int. Ed.* **2012**, *51*, 3822−3825.
(31) Ercolani, C.; Gardini, M.; Pennesi, G.; Rossi, G.; Russo, U. High-valent iron phthalocyanine μ-nitrido dimer. *Inorg. Chem.* **1988**, *27*, 422−424.
(32) Yamada, Y.; Sugiura, T.; Morita, K.; Ariga-Miwa, H.; Tanaka, K. Improved synthesis of monocationic μ-nitrido-bridged iron phthalocyanine dimer with no peripheral substituents. *Inorg. Chim. Acta* **2019**, *489*, 160−163.
(33) Huang, Y. L.; Chen, W.; Chen, S.; Wee, A. T. S. Low-temperature scanning tunneling microscopy and near-edge X−ray absorption fine structure investigation of epitaxial growth of F_{16}CuPc thin films on graphite. *Appl. Phys. A* **2009**, *95*, 107−111.
(34) Stöhr, J.*NEXAFS Spectroscopy*; Springer: Berlin, 1992.
(35) Hammond, C.; Forde, M. M.; Ab Rahim, M. H.; Thetford, A.; He, Q.; Jenkins, R. L.; Dimitratos, N.; Lopez-Sanchez, J. A.; Dummer, N. F.; Murphy, D. M.; Carley, A. F.; Taylor, S. H.; Willock, D. J.; Stangland, E. E.; Kang, J.; Hagen, H.; Kiely, C. J.; Hutchings, G. J. Direct catalytic conversion of methane to methanol in an aqueous medium by using copper-promoted Fe-ZSM-5. *Angew. Chem., Int. Ed.* **2012**, *51*, 5129−5133.
(36) Yamada, Y.; Kura, J.; Toyoda, Y.; Tanaka, K. μ−Nitrido-bridged iron phthalocyanine dimer bearing eight peripheral 12-crown-4 units and its methane oxidation activity. *New J. Chem.* **2020**, *44*, 19179−19183.
(37) Yamada, Y.; Miwa, Y.; Toyoda, Y.; Yamaguchi, T.; Akine, S.; Tanaka, K. Synthesis of a monomeric μ−nitrido−bridged iron porphycene dimer and its methane oxidation activity. *Dalton Trans.* **2021**, *50*, 16775−16781.
(38) Ghosh, A.; Mitchell, D. A.; Chanda, A.; Ryabov, A. D.; Popescu, D. L.; Upham, E. C.; Collins, G. J.; Collins, T. J. Catalase-peroxide activity of iron(III)-TAML activators of hydrogen peroxide. *J. Am. Chem. Soc.* **2008**, *130*, 15116−15126.
(39) Liu, J.; Cui, L.; Losic, D. Graphene and graphene oxide as new nanocarriers for drug delivery applications. *Acta Biomater.* **2013**, *9*, 9243−9257.
(40) Han, B.; Zhang, Y. -L.; Chen, Q. -D.; Sun, H. -B. Carbon-based photothermal actuators. *Adv. Funct. Mater.* **2018**, *28*, 1802235.
(41) Nagababu, P.; Yu, S. S. -F.; Maji, S.; Ramu, R.; Chan, S. I. Developing an efficient catalyst for controlled oxidation of small alkanes under ambient conditions. *Catal. Sci. Technol.* **2014**, *4*, 930−935.
(42) Bottomley, L. A.; Gorce, J.-N.; Goedken, V. L.; Ercolani, C. Spectroelectrochemistry of a μ-nitrido-bridged iron phthalocyanine dimer. *Inorg. Chem.* **1985**, *24*, 3733−3737.
(43) Trasatti, S. The absolute electrode potential: an explanatory note. *Pure Appl. Chem.* **1986**, *58*, 955−966.
(44) Akada, K.; Obata, S.; Saiki, K. Work function lowering of graphite by sequential surface modifications: nitrogen and hydrogen plasma treatment. *ACS Omega* **2019**, *4*, 16531−16535.
(45) Feng, S.; Luo, N.; Tang, A.; Chen, W.; Zhang, Y.; Huang, S.; Dou, W. Phthalocyanine and metal phthalocyanines adsorbed on graphene: a density functional study. *J. Phys. Chem. C* **2019**, *123*, 16614−16620.
(46) Ercolani, C.; Gardini, M.; Goedken, V. L.; Pennesi, G.; Rossi, G.; Russo, U.; Zanonato, P. High-valent iron phthalcyanine five- and six-coordinated μ-carbido dimers. *Inorg. Chem.* **1989**, *28*, 3097−3099.
(47) Colomban, C.; Kudrik, E. V.; Briois, V.; Shwarbrick, J. C.; Sorokin, A. B.; Afanasiev, P. X-ray absorption and emission spectroscopies of X-bridged diiron phthalocyanine complexes $(FePc)_2X$ (X = C, N, O) combined with DFT study of $(FePc)_2X$ and their high-valent diiron oxo complexes. *Inorg. Chem.* **2014**, *53*, 11517−11530.
(48) Shimizu, T.; Wakamatsu, K.; Yamada, Y.; Toyoda, Y.; Akine, S.; Yoza, K.; Yoshikawa, H. Application of μ−nitride− and μ−carbido−bridged iron phthalocyanine dimers as cathode-active materials for rechargeable batteries. *ACS Appl. Mater. Interfaces* **2021**, *13*, 40612−40617.
(49) Yamaguchi, K.; Watanabe, Y.; Morishima, I. Push effect on the heterolytic O−O bond vcleavage of peroxoiron(III) porphyrin adducts. *Inorg. Chem.* **1992**, *31*, 156−157.
(50) Ho, S. S. H.; Yu, J. Z. Feasibility of collection and analysis of airborne carbonyls by on-sorbent derivatization and thermal desorption. *Anal. Chem.* **2002**, *74*, 1232−1240.

https://doi.org/10.1021/jacsau.2c00618
JACS Au 2023, 3, 823−833